INFRARED PHYSICS & TECHNOLOGY

Aims and Scope: The journal covers the whole field of infrared physics and technology: theory, experiment, devices and instrumentation. Its core topics can be summarized as the generation, propagation and detection of infrared radiation; the associated optics, materials and devices; and its use in all fields of science, industry and medicine and engineering.
Editorial Office: Elsevier Science B.V., P.O. Box 2759, 1000 CT Amsterdam, The Netherlands. Tel.: +31 20 4852638; Fax: +31 20 4852319; E-mail: F.KOP@ELSEVIER.NL.
Subscription Information 1998: Infrared Physics & Technology (ISSN 1350-4495) appears in 7 issues per annum, in February, March, April, June, August, October and December. Subscriptions are accepted on a prepaid basis only and are entered on a calendar year basis. Issues are sent by SAL (Surface Air Lifted) mail wherever this service is available. Airmail rates are available upon request. For orders, claims, product enquiries (no manuscript enquiries) please contact the Customer Support Department at the Regional Sales Office nearest to you:
New York, Elsevier Science, P.O. Box 945, New York, NY 10159-0945, USA. Tel.: +1 212 633 3730 [Toll Free number for North American customers: 1 888 4ES INFO (437 4636)]; Fax: +1 212 633 3680; E-mail: usinfo-f@elsevier.com.
Amsterdam, Elsevier Science, P.O. Box 211, 1000 AE Amsterdam, The Netherlands. Tel.: +31 20 485 3757; Fax: +31 20 485 3432; E-mail: nlinfo-f@elsevier.nl.
Tokyo, Elsevier Science, 9-15, Higashi-Azabu 1-chome, Minato-ku, Tokyo 106, Japan. Tel.: +81 3 5561 5033; Fax: +81 3 5561 5047; E-mail: info@elsevier.co.jp.
Singapore, Elsevier Science, No. 1 Temasek Avenue, #17-01 Millenia Tower, Singapore 039192. Tel.: +65 434 3727; Fax: +65 337 2230; E-mail: asiainfo@elsevier.com.sg.
Claims for issues received should be made within six months of our publication (mailing) date.
Abstracted/Indexed in: Current Contents: Physical, Chemical & Earth Sciences.

USA mailing info – Infrared Physics & Technology (ISSN 1350-4495) is published monthly except January, May, July, September, November (total seven issues) by Elsevier Science B.V. (P.O. Box 211, 1000 AE Amsterdam). Annual subscription price in the USA US$ 1039.00 (valid in North, Central and South America), including air speed delivery. Application to mail at periodicals postage rate is pending at Jamaica, NY 11431.
USA POSTMASTER: Send address changes to Infrared Physics and Technology Publications Expediting Inc., 200 Meacham Ave, Elmont, NY 11003. AIRFREIGHT AND MAILING in the USA by Publications Expediting Inc., 200 Meacham Ave, Elmont, NY 11003.

♾ The paper used in this publication meets the requirements of ANSI/NISO Z39.48-1992 (Permanence of Paper).

Printed in The Netherlands

North-Holland, an imprint of Elsevier Science

ELSEVIER

Infrared Physics & Technology 39 (1998) 203–211

INFRARED PHYSICS & TECHNOLOGY

Optical properties of ALON (aluminum oxynitride)

T.M. Hartnett *, S.D. Bernstein, E.A. Maguire, R.W. Tustison

Raytheon Electronic Systems, Lexington Laboratory, 131 Spring St., Lexington, MA 02173, USA

Abstract

The optical properties of ALON (aluminum oxynitride) are presented. Optical scatter and index of refraction, and absorption of several different compositions of ALON are compared. The temperature dependence of emissivity of ALON was measured in the temperature range 46°C to 1200°C.

Keywords: ALON, aluminum oxynitride; Optical properties; Scatter; Spectral emittance

1. Introduction

Aluminum oxynitride or ALON is a polycrystalline ceramic material of high strength and hardness. This material is made by conventional sintering and hot pressing of a powder compact. Powder compacts of near net shape have been made by isostatic pressing, by slip casting, and by injection molding methods of forming. Full density and intrinsic transparency extending from ultraviolet wavelengths (UV) to mid-infrared wavelengths (MID-IR) have been achieved.

The performance of ALON windows in an optical system will depend on the scatter which can cause a reduction in signal-to-noise and degradation in image resolution. ALON has the cubic [spinel] crystal structure. The optical properties of ALON are therefore isotropic and a polycrystalline ALON ceramic will not scatter light due to birefringence. Scattering due to other sources is present in ALON and recent developments have led to lower scatter levels than have previously been achieved.

In applications where the material will become hot due to aerodynamic heating the emittance of ALON becomes important. IN this paper, recent measurements of scatter in ALON at several wavelengths from the UV to the MID-IR and spectral emittance measurements made from room temperature to 1200°C will be presented.

Measurements of the variation of the refractive index with composition and wavelength are also presented. A comparison of the values of the refractive index, dn/dt, scatter and emissivity from the literature is made.

2. Composition range of cubic ALON

The stability range for the spinel phase, ALON, in the $AlN–Al_2O_3$ system is outside the ideal $9AL_2O_3 \cdot 5AlN$ composition (35.7 mol % AlN). The constant anion model of McCauley [1] and Lejus [2] for the spinel crystal structure given in Eq. (1) describes the

* Corresponding author.
E-mail: thomas_m_hartnett@ raytheon.com.

1350-4495/98/$19.00
PII S1350-4495(98)00007-3

defect structure of ALON. In this equation Al is aluminum, V is cation lattice vacancy, O is oxygen, and N is nitrogen. The composition range of stability for single-phase ALON was determined to extend from 5.52 at.% nitrogen (23.7 mol % AlN) to 8.20 percent nitrogen (32.9 mole % AlN).

$$Al_{(64+x)/3}V_{(8-x)/3}O_{32-x}N_x \quad (1)$$

Fig. 1 graphs the lattice constant of cubic ALON vs. nitrogen content. The relationship between lattice constant and nitrogen content was determined using the constant anion model of Eq. (1) in conjunction with X-ray diffraction measurements of the lattice constant and density measurements. Chemical analysis of the nitrogen content of ALON was performed by inert gas fusion (accurate to $\pm 0.1\%$ nitrogen) to verify the composition determined by X-ray diffraction and density measurements. Corbin [3] provides an excellent review of previous work on the composition range of stability of ALON and other phases that can form in the $AlN–Al_2O_3$ system.

The useful transmission range of ALON extends from 0.22 μm to 5.2 μm. The long wavelength cutoff as a function of composition was determined by measuring the transmission of two sample of thickness and calculating the extinction coefficient. The extinction coefficient in the infrared cutoff region increases with increasing nitrogen content as shown in Fig. 2. Higher temperatures will shift the infrared cutoff to shorter wavelengths. Joseph et al. [4] have developed a multiphonon absorption model for ALON and several other oxide window materials (e.g., sapphire, yttria, and spinel). In their paper they presented the absorption coefficient of these materials as a function of temperature and wavelength in the infrared cutoff region. Later in this paper we present high temperature spectral emittance measurements of ALON.

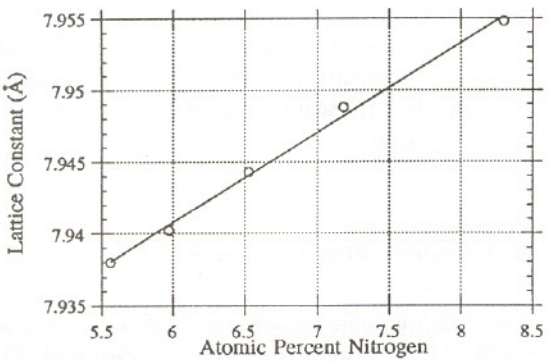

Fig. 1. Variation of the lattice constant of single phase ALON with nitrogen content. Lattice constant = 7.9032 + 0.00625 × (at.% nitrogen).

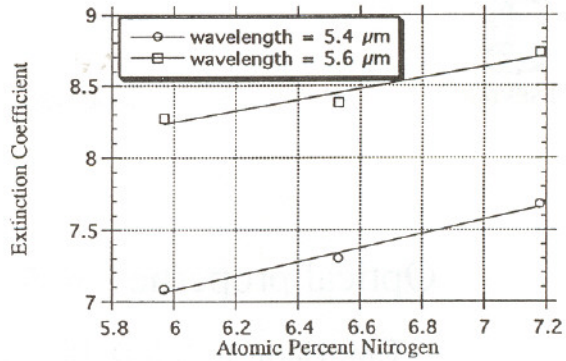

Fig. 2. Extinction coefficient of ALON vs. composition in the infrared cutoff.

3. Optical scatter in ALON

The reduction in optical scatter in transparent polycrystalline materials like ALON is very important in for improving the performance of an optical system. The most detrimental effects of scatter are a reduced signal-to-noise ratio and reduced image resolution. Unlike glass materials such as calcium aluminate or single crystal materials such as sapphire ALON contains grain boundaries. Since ALON has cubic symmetry and is optically isotropic, scattering due to the refractive index difference along different crystallographic directions is not a contributor to optical scatter. Grain boundaries as well as the individual grains themselves are, however, potential scattering sites for the following reasons: (1) refractive index variations due to composition variations at grain boundaries; (2) refractive index variations due to composition variations between adjacent grains; (3) structural defects (dislocations, twins, stacking faults) located at grain boundaries; (4) particulate inclusions of noncubic ALON phase or aluminum

Table 1
Comparison of scatter in ALON

Sample	Grain size (μm)	CTIS from 2.5° to 90° at wavelength indicated		
		0.6328 μm	1.06 μm	3.39 μm
ALON (Sample C1)	151	0.15%	0.1%	0.078%
ALON (Sample C)	84	2.72%	3.55%	5.5%

nitride; (5) refractive index variations due to composition variations due to strain.

In addition to these bulk scattering sources, there is also a contribution to the total scatter due to surface scattering. Differences in polishing rates at grain boundaries and at twin boundaries can result in a grain relief structure at the surface which will cause scatter. A comparison of surface scattering and bulk scattering has not yet been made for ALON.

The optical scatter and imaging performance of ALON and several other polycrystalline oxides and single crystal sapphire has been described previously by Duncan et al. [5]. Reduction of the optical scatter in ALON has been made since their study and these recent measurements will be examined here. Scatter measurements on ALON test samples was performed at TMA Technologies (Bozeman, MT). Details of the measurement technique are given by Stover [6]. The bidirectional transmissive scatter distribution function (BTDF) was measured at several laser wavelengths. Using this method, the angular distribution of the optical scatter is measured and calculated total integrated scatter (CTIS) can be obtained. In this paper the effect of grain size on scatter will be examined at wavelengths from the UV (325 nm) to IR (3.39 μm).

ALON samples of two grain sizes were prepared for scatter measurements. Both large- and small-grained samples are compared in Table 1. Samples C (small size) and C1 (large grain size) are ALON samples having grain sizes of 84 μm and 150 μm, respectively.

The scatter from ALON exhibits a maximum in scattered intensity close to the specular beam. Increased grain size shifts this maximum in scattered intensity to smaller angles. In Fig. 3 the angular distribution of scatter is compared for samples C and C1 measured at 3.39 μm. The maximum in scattered intensity can be seen for sample C. A similar comparison can be made for other wavelengths with the maximum shifting to smaller angles with decreasing wavelength. In Table 2 the location of the maximum in scattered intensity is shown for sample as a function of wavelength. Fig. 4 plots the angle at which the maximum occurs as a function of wavelength. Assuming the scattered light intensity maximum results from a diffraction effect with an Airy distribution, the particle size of the scattering sites can be calculated from Eq. (2) [5].

$$\text{angle (radians)} = 1.635\lambda/D \qquad (2)$$

where: λ is the wavelength, D is the size of the scattering site.

For sample C the calculated size of the scattering sites is 65 μm and the measured grain size 84 μm.

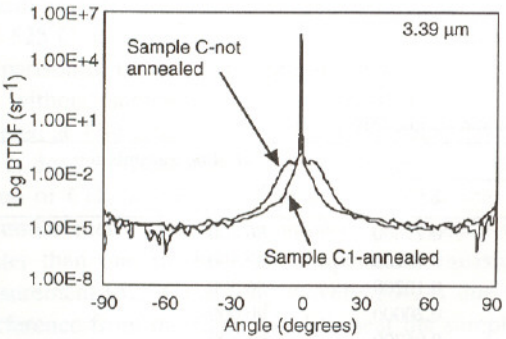

Fig. 3. Comparison of the measured BTDF for samples C and C1 of ALON (measured at a wavelength of 3.39 μm).

Table 2
Angular location of the maximum in scattered intensity

Wavelength	Angle (sample C)
3.3900	4.86°
1.0600	1.58°
0.63280	1.05°

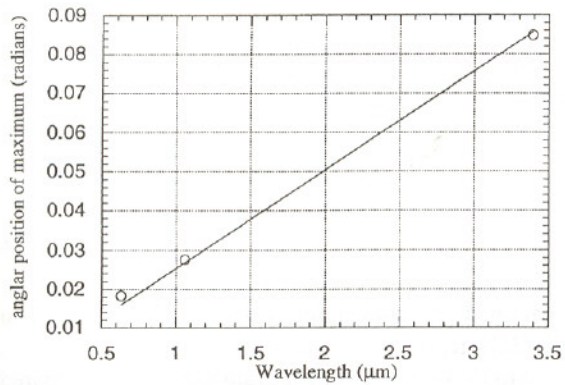

Fig. 4. Angle of maximum scattered light intensity vs. wavelength for C.

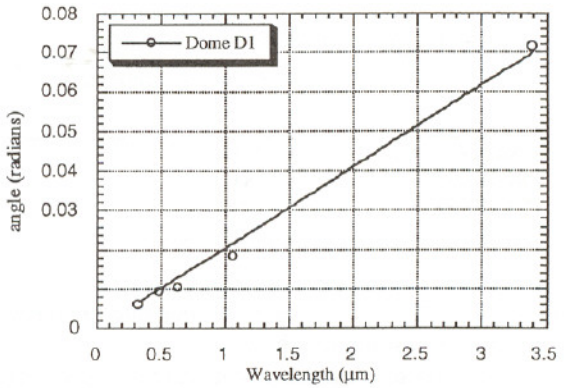

Fig. 5. Angle of maximum scattered light intensity vs. wavelength for dome sample D1.

The calculated size of the scattering sites is on the order of the grain sizes. The location of the maximum in the scattered intensity distribution vs. angle moves to smaller angles and the magnitude of the maximum decreases substantially. The measured grain size of sample C1 is 151 μm. Scattering sites of this size would move the maximum in scattered intensity to about 2.1% for sample C1.

Scatter was measured on a hemispherical ALON dome at five wavelengths in the UV to MID-IR spectral region. This dome was anti-reflection coated on one side after polishing. On this sample more precise measurements were made close to the specular direction than for the previous flat samples C and C1. Table 3 compares the angular and wavelength dependence of scatter from this 'low scatter' ALON dome (sample dome D1, 0.050 in. thick). As indicated in this table a much higher degree of scatter is measured within 0.5° of the specular direction and decreases dramatically beyond 0.5°. The angular location of the maximum in scattered intensity vs. wavelength for ALON dome D1 is shown in Fig. 5. Fitting this data to Eq. (1) the size of the scattering site is found to be 80 μm. The CTIS calculated from 0.1° to 90° has a wavelength dependence that is proportional to the inverse 2.5 power of the wavelength $(1/\lambda^{2.5})$ as shown in Fig. 6. This indicates that the scattering sites are larger than the wavelength of the light used which is consistent with the scattering site being on the order of the grain size.

4. Emittance measurements

Emittance measurements were made on a polished ALON sample having a 1-in. diameter and a 0.0775-

Table 3
Comparison of the angular and wavelength dependence of scatter in ALON dome sample D1[a]

Wavelength	CTIS (% integrated scatter from angle indicated to 70°)				% In-line transmission
	0.1°	0.5°	1.0°	2.5°	
325 nm	9.0000	3.6800	0.64800	0.29600	86.400
488 nm	3.0900	2.3800	0.70600	0.19200	89.500
633 nm	1.9000	1.3800	0.66500	0.10200	86.500
1.08 μm	0.63100	0.56800	0.54000	0.20000	90.000
3.39 μm	0.07800	0.06200	0.06200	0.05700	91.800

[a]This sample was anti-reflection coated on one side and has a higher transmission at selected wavelengths than would uncoated ALON.

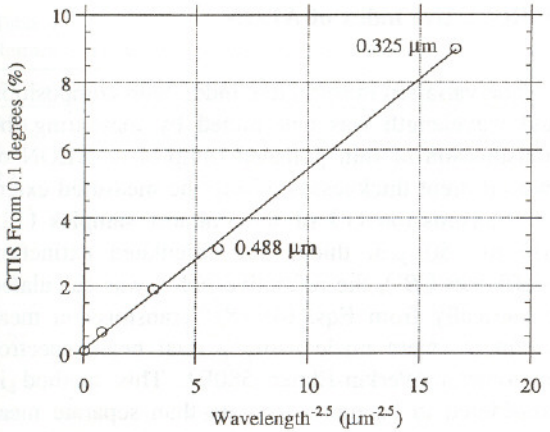

Fig. 6. Wavelength dependence of scatter in ALON.

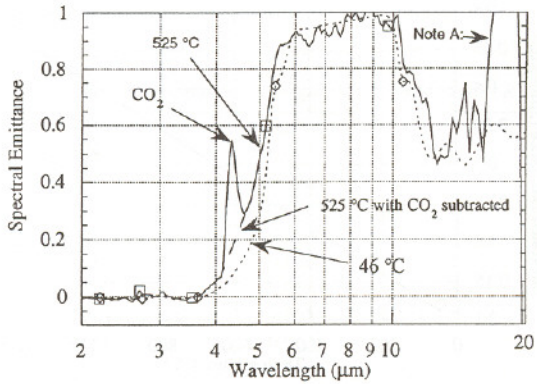

Fig. 7. Spectral emission of ALON at 46°C and at 525°C. A comparison of the spectra with and without subtraction of the CO_2 peak centered at 4.34 μm. Note A: The apparent emittance of greater than one is due to interference from the flame used to heat the sample.

in. thickness. The measurements were performed by Advanced Fuel Research (East Hartford, CT). Spectra were measured at 32 cm^{-1} resolution using a Bomem M151 FTIR spectrometer. In the method used, the directional–hemispherical transmittance ($\tau\lambda$), the directional–hemispherical reflectance ($\rho\lambda$) and the sample radiance (R_1) are measured. The spectral emittance ($\varepsilon\lambda$) is obtained from the relationship:

$$\varepsilon\lambda = 1 - \tau\lambda - \rho\lambda \tag{3}$$

In the technique used, the measured radiance and the spectral emittance are used to determine the sample surface temperature. A complete description of the measurement technique is described in detail in Refs. [7,8].

The spectral emittance of ALON in the 2 μm to 20 μm wavelength region at temperatures of 46°C and 525°C is shown in Fig. 7. In this figure a comparison of the measured emittance at 525°C with and without subtraction of the broad CO_2 peak centered at 4.34 μm is shown. The CO_2 peak at 4.34 μm is due to differences in the background concentration of CO_2 in the air in an unpurged section of the emissometer setup. The apparent emittance of greater than one in the high temperature emission measurement (525°C) at long wavelengths is due to interference from the flame used to heat the sample.

The region of interest for ALON is the 3 μm to 5 μm wavelength region. Fig. 8 compares the emittance of ALON at three temperatures (the CO_2 peak at 4.34 μm has been subtracted from these spectra). In Fig. 9 the integrated spectral emittance over the wavelength band 3 μm to 5 μm are plotted vs. temperature. In Fig. 10 the dependence of spectral emmittance on temperature is shown for several wavelengths in the 3 μm to 5 μm wavelength region. The rapid increase in emittance at increasing wavelengths greater than 4 μm is apparent from these graphs. The useful range of ALON as an optical window in applications where the window will be heated are limited to wavelengths shorter than about 4 μm.

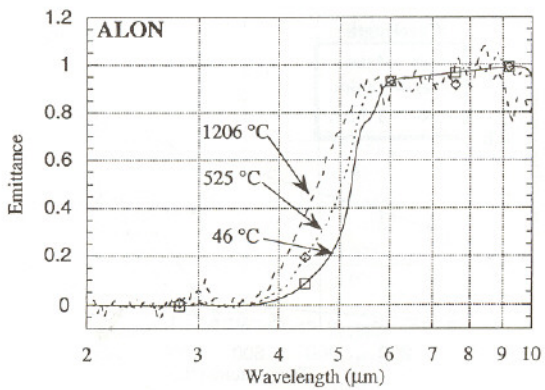

Fig. 8. Spectral emittance of ALON at several temperatures in the 2 μm to 10 μm wavelength region.

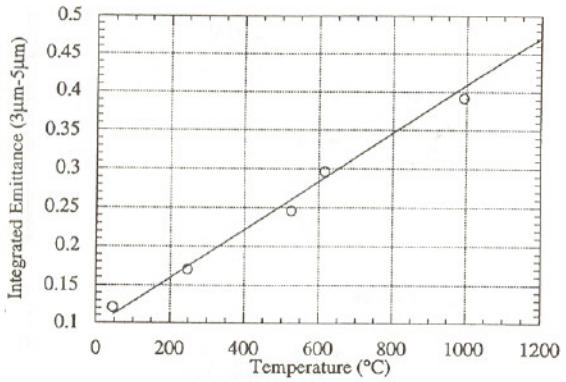

Fig. 9. Integrated emittance of ALON vs. temperature in the 3 μm to 5 μm wavelength region.

Sova et al. [9] measured the emissivity of several oxide dome materials. ALON was measured at 687°C and the measured results compared with a theoretical model. The measured data of Sova et. al. is plotted on Fig. 10 in comparison with the current measured values. The difference between the two may be due to the interference of the CO_2 peak in this wavelength of interest. Sova et. al. used a completely purged system so the influence of atmospheric CO_2 was not a factor. Also, they used laser heating of the sample rather than a flame. The flame method of heating can also introduce CO_2 as well as water vapor from the burning of fuel and oxygen.

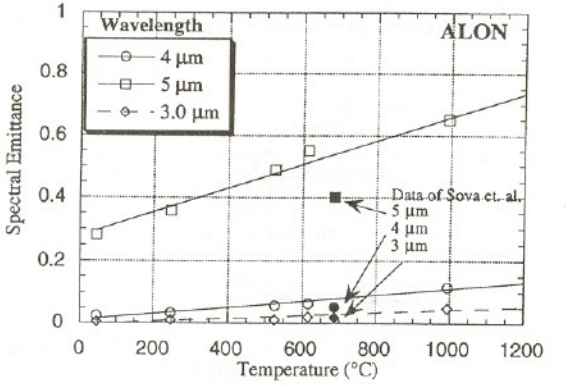

Fig. 10. Spectral emittance of ALON vs. temperature for several wavelengths in the 3 μm to 5 μm spectral region.

5. Refractive index of ALON

The variation in refractive index with composition and wavelength was determined by measuring the transmission of thin polished samples of ALON of two different thicknesses. Using the measured external transmission (τ) of the thinnest samples (125 μm to 150 μm thick) and calculated extinction coefficient (β'), the refractive index was calculated numerically from Eqs. (4)–(8). Transmission measurements were made using a dual beam spectrophotometer (Perkin-Elmer 580B). This method is considered to be more accurate than separate measurements of transmission and reflection because of the greater accuracy of the instrument in measuring transmission compared to reflection.

$$\tau = \frac{(1-R)^2 T}{1-R^2T^2} \qquad \text{external transmission} \qquad (4)$$

$$T = \exp(-\beta' t) \qquad \text{internal transmission} \qquad (5)$$

$$R = \frac{(n-1)^2 + k^2}{(n+1)^2 + k^2} \qquad \text{single surface reflectance} \qquad (6)$$

$$k = \frac{\beta'\lambda}{4\pi} \qquad \text{index of absorption} \qquad (7)$$

$$\beta' = -\frac{\ln\left(\frac{\tau_2}{\tau_1}\right)}{(t_2 - t_1)} \qquad \text{extinction coefficient} \qquad (8)$$

where: t is the sample thickness, n is the refractive index, λ is the wavelength.

The variation in refractive index with composition and wavelength is shown in Tables 4–7. A comparison of the high and low nitrogen contents ($a_o = 7.948$ Å and $a_o = 7.940$ Å) indicates an increase in the refractive index with increasing nitrogen content over the entire wavelength range. The intermediate composition ($a_o = 7.944$ Å) shows a smaller index of refraction than the $a_0 = 7.940$ Å composition in the UV visible and near IR spectral region to 1 μm and then follows the trend established by the high and the low compositions at longer IR wavelengths. This may be due to lower scatter in this sample than in

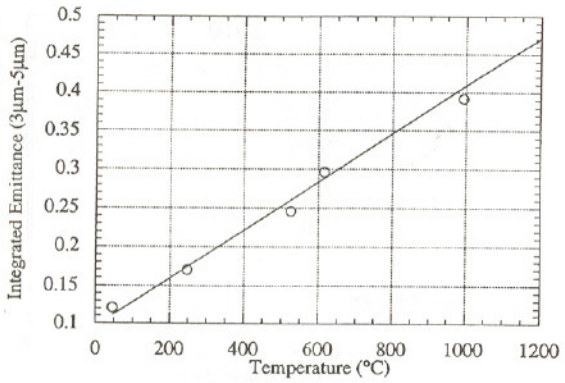

Fig. 9. Integrated emittance of ALON vs. temperature in the 3 μm to 5 μm wavelength region.

Sova et al. [9] measured the emissivity of several oxide dome materials. ALON was measured at 687°C and the measured results compared with a theoretical model. The measured data of Sova et. al. is plotted on Fig. 10 in comparison with the current measured values. The difference between the two may be due to the interference of the CO_2 peak in this wavelength of interest. Sova et. al. used a completely purged system so the influence of atmospheric CO_2 was not a factor. Also, they used laser heating of the sample rather than a flame. The flame method of heating can also introduce CO_2 as well as water vapor from the burning of fuel and oxygen.

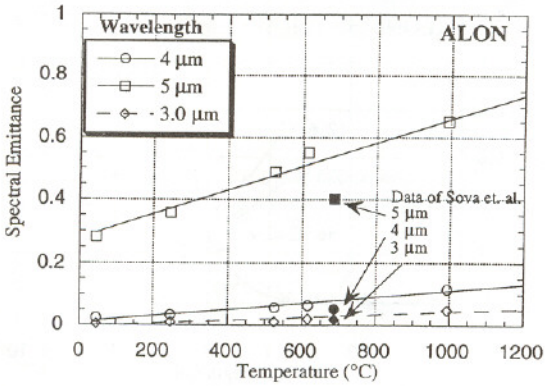

Fig. 10. Spectral emittance of ALON vs. temperature for several wavelengths in the 3 μm to 5 μm spectral region.

5. Refractive index of ALON

The variation in refractive index with composition and wavelength was determined by measuring the transmission of thin polished samples of ALON of two different thicknesses. Using the measured external transmission (τ) of the thinnest samples (125 μm to 150 μm thick) and calculated extinction coefficient (β'), the refractive index was calculated numerically from Eqs. (4)–(8). Transmission measurements were made using a dual beam spectrophotometer (Perkin-Elmer 580B). This method is considered to be more accurate than separate measurements of transmission and reflection because of the greater accuracy of the instrument in measuring transmission compared to reflection.

$$\tau = \frac{(1-R)^2 T}{1-R^2T^2} \qquad \text{external transmission} \qquad (4)$$

$$T = \exp(-\beta' t) \qquad \text{internal transmission} \qquad (5)$$

$$R = \frac{(n-1)^2 + k^2}{(n+1)^2 + k^2} \qquad \text{single surface reflectance} \qquad (6)$$

$$k = \frac{\beta'\lambda}{4\pi} \qquad \text{index of absorption} \qquad (7)$$

$$\beta' = -\frac{\ln\left(\frac{\tau_2}{\tau_1}\right)}{(t_2 - t_1)} \qquad \text{extinction coefficient} \qquad (8)$$

where: t is the sample thickness, n is the refractive index, λ is the wavelength.

The variation in refractive index with composition and wavelength is shown in Tables 4–7. A comparison of the high and low nitrogen contents ($a_o = 7.948$ Å and $a_o = 7.940$ Å) indicates an increase in the refractive index with increasing nitrogen content over the entire wavelength range. The intermediate composition ($a_o = 7.944$ Å) shows a smaller index of refraction than the $a_0 = 7.940$ Å composition in the UV visible and near IR spectral region to 1 μm and then follows the trend established by the high and the low compositions at longer IR wavelengths. This may be due to lower scatter in this sample than in

Table 4
Refractive index and extinction coefficient for ALON (lattice constant $a_o = 7.940$ Å)

Wavelength (μm)	Index of refraction (n)	Extinction coefficient (β')	External transmittance	Single surface refl
0.24	1.914	3.121	0.7901	0.0984
0.34	1.825	0.194	0.8408	0.0853
0.4	1.807	0.151	0.8458	0.0827
0.6	1.779	0.115	0.8530	0.0786
1	1.749	0.081	0.8610	0.0742
2.8	1.722	0.047	0.8681	0.0703
3.4	1.706	0.035	0.8721	0.0681
4	1.685	0.161	0.8761	0.0651
4.6	1.660	0.731	0.8761	0.0616
5	1.653	1.576	0.8690	0.0606
5.4	1.607	7.084	0.8230	0.0546
5.6	1.586	8.271	0.8159	0.0518

Table 5
Refractive index and extinction coefficient for ALON (lattice constant $a_o = 7.944$ Å)

Wavelength (μm)	Index of refraction (n)	Extinction coefficient (β')	External transmittance (τ)	Single surface reflectance (R)
0.24	1.907	2.862	0.7900	0.0973
0.34	1.820	0.208	0.8416	0.0846
0.4	1.804	0.162	0.8462	0.0822
0.6	1.770	0.128	0.8550	0.0772
1	1.748	0.084	0.8611	0.0741
2.8	1.722	0.108	0.8671	0.0704
3.4	1.709	0.044	0.8711	0.0686
4	1.692	0.159	0.8742	0.0660
4.6	1.671	0.729	0.8722	0.0632
5	1.656	1.598	0.8652	0.0612
5.4	1.618	7.300	0.8070	0.0562
5.6	1.604	8.383	0.7979	0.0543

Table 6
Refractive index and extinction coefficient for ALON (lattice constant $a_o = 7.948$ Å)

Wavelength (μm)	Index of refraction (n)	Extinction coefficient (β')	External transmittance (τ)	Single surface reflectance (R)
0.24	1.929	6.353	0.7411	0.1006
0.34	1.838	0.194	0.8370	0.0873
0.4	1.821	0.151	0.8420	0.0846
0.6	1.782	0.115	0.8520	0.0790
1	1.760	0.081	0.8580	0.0758
2.8	1.747	0.047	0.8617	0.0740
3.4	1.738	0.035	0.8640	0.0727
4	1.712	0.161	0.8688	0.0690
4.6	1.694	0.731	0.8657	0.0664
5	1.671	1.589	0.8600	0.0632
5.4	1.628	7.684	0.7929	0.0576
5.6	1.616	8.735	0.7830	0.0559

Table 7
Comparison of the variation of the refractive index of ALON with composition and wavelength

Wavelength (μm)	Index of refraction (n) $a_o = 7.940$ 5.88 at.% N	Index of refraction (n) $a_o = 7.944$ 6.53 at.% N	Index of refraction (n) $a_o = 7.948$ 7.17 at.% N	Sellmeier formula index calculation $a_o = 7.945$ Å 6.69 at.% N
0.24	1.914	1.907	1.929	1.901
0.34	1.825	1.820	1.838	1.830
0.4	1.807	1.804	1.821	1.813
0.6	1.779	1.770	1.782	1.788
1	1.749	1.748	1.760	1.774
2.8	1.722	1.722	1.747	1.743
3.4	1.706	1.709	1.738	1.728
4	1.685	1.692	1.712	1.710
4.6	1.660	1.671	1.694	1.688
5	1.653	1.656	1.671	1.671
5.4	1.607	1.618	1.628	1.652
5.6	1.586	1.604	1.616	1.642

the other two compositions. In the refractive index calculations the separate effects of scatter and absorption are grouped together in the extinction coefficient (β'). This may cause a small error in the index calculation for the more highly scattering samples at shorter wavelengths.

The refractive index of ALON has been measured by R.J. Scheller of Schott Glass Technologies, using an ALON prism by Raytheon. The Sellmeier formula determined from these measurements is given in Eq. (9). The composition of this sample based on a lattice constant of 7.945 Å is 6.69 at.% nitrogen. Tropf and Thomas [10] compiled a table of refractive index values (n and k) for ALON based on the measurements of Scheller and theoretical models. A comparison of the values measured by transmission measurements and calculated values using the Sellmeier formula given in Eq. (9) is given in Table 7.

Measurements of the variation in the refractive index with temperature were made by several researchers. Lange and Duncan [11] determined the temperature coefficient of refractive index (dn/dT) using measurements of optical path length difference as a function of temperature in a Michelson interferometer at a wavelength of 0.633 μm from room temperature to 500°C. Included in this reference is a comparison of dn/dT for ALON with several other oxides. A value of $1.46 \pm 0.1 \times 10^{-5}$/°C was obtained. Tropf and Thomas measured a value of 1.5×10^{-5}/°C at 0.6328 μm and calculated a value of 2.8×10^{-6} at 4.0 μm [10].

The Sellmeier formula determined for ALON is:

$$n^2 - 1 = \frac{20.32 \times 10^9}{(97{,}500)^2 - v^2} + \frac{1.287 \times 10^6}{(530)^2 - v^2} \qquad (9)$$

6. Summary

Polycrystalline aluminum oxynitride with its cubic Spinel crystal structure is a very durable optical material with a high degree of transparency from the UV to the mid-IR wavelengths. Minimization of grain boundary defects reduces optical scatter significantly. Levels of scatter of about 0.1% can be achieved.

Emittance of the material is an important factor in situations where elevated temperatures are encountered. ALON experiences a rapid emittance increase at wavelengths greater than about 4 μm. there is a linear relationship to temperature in the 3 μm to 5 μm region.

Refractive index varies with wavelength and with composition of the ALON. A Sellmeier formula has been derived. The temperature coefficient of refractive index has been measured as 1.5×10^{-5}/°C.

References

[1] J.W. McCauley, J. Am. Ceram. Soc. 61 (7–8) (1978) 372.

[2] A.M. Lejus, Sur la formation a haute temperature de spinelles non stoetechiometriques et de phase derivees, Rev. Hautes Temp. Refract. 1 (1964) 80–95.

[3] N.D. Corbin, Aluminum oxynitride spinel, Int. J. High Technol. Ceram. 5 (3) (1989) 143–154, (a review).

[4] M.E. Thomas, R.I. Joseph, W.J. Tropf, Infrared transmission properties of sapphire, spinel, yttria, and ALON as a function of temperature and frequency, Appl. Optics 27 (2) (1988) 239–245.

[5] D.D. Duncan, C.H. Lange, D.G. Fischer, Proc. SPIE 1326 (1990) 95.

[6] J.C. Stover, Lasers and Optronics, August (1988).

[7] J.R. Markham, P.R. Solomon, P.E. Best, Rev. Sci. Ins 61 (1990) 3700.

[8] J.R. Markham, K. Kinsella, R.M. Carangelo, C.A. B lette, M.D. Carangelo, P.E. Best, P.R. solomon, Rev Instrum. 64 (1993) 2515.

[9] R.M. Sova, M.J. Linevsky, M.E. Thomas, F.F. Mark, temperature optical properties of oxide dome materials, SPIE 1760 Windows and Dome Technologies and Mat III, 1992, p. 27.

[10] W.J. Tropf, M.E. Thomas, in: E.D. Palik (Ed.), Handbo Optical Constants of Solids II, Academic Press, B (1991), p. 77.

[11] C.H. Lange, D.D. Duncan, Temperature coefficient of r tive index for candidate optical windows, Proc. SPIE Windows and Dome Technologies and Materials II, 19 71.

Reprinted from

INFRARED PHYSICS & TECHNOLOGY

Infrared Physics & Technology 39 (1998) 203–211

Optical properties of ALON (aluminum oxynitride)

T.M. Hartnett *, S.D. Bernstein, E.A. Maguire, R.W. Tustison

Raytheon Electronic Systems, Lexington Laboratory, 131 Spring St., Lexington, MA 02173, USA

ELSEVIER